small method
www.small-methods.com

Pd-Ru Alloy Nanocages with a Face-Centered Cubic Structure and Their Enhanced Activity toward the Oxidation of Ethylene Glycol and Glycerol

*Ming Zhao, Zhiheng Lyu, Minghao Xie, Zachary D. Hood, Zhenming Cao, Miaofang Chi, and Younan Xia**

This article reports a facile method for the synthesis of Pd-Ru nanocages by activating the galvanic replacement reaction between Pd nanocrystals and a Ru(III) precursor with I^- ions. The as-synthesized nanocages feature a hollow interior, ultrathin wall of ≈2.5 nm in thickness, and a cubic shape. Our quantitative study suggests that the reduction rate of the Ru(III) precursor can be substantially accelerated upon the introduction of I^- ions and then retarded as the ratio of I^-/Ru^{3+} is increased. The Pd-Ru nanocages take an alloy structure, with the Ru atoms in the nanocages crystallized in a face-centered cubic structure instead of the hexagonal close-packed phase taken by bulk Ru. Using Pd nanocubes with different edge lengths, the dimensions of the nanocages in the range of 6–18 nm can readily be tuned. When tested as catalysts toward the electro-oxidation of ethylene glycol and glycerol, respectively, the Pd-Ru cubic nanocages prepared from 18 nm Pd cubes exhibit 5.1- and 6.2-fold enhancements in terms of mass activity relative to the commercial Pd/C. After 1000 cycles of accelerated durability test, the mass activities of the nanocages are still 3.3 and 3.7 times as high as that of the pristine commercial Pd/C catalyst, respectively.

1. Introduction

As a class of clean-energy devices, direct methanol fuel cells (DMFCs) are attractive for powering portable devices and transportation vehicles. In contrast to the H_2-based fuel cells, DMFCs offer multiple advantages such as easy storage, transport, and refueling of fuels, in addition to a superior volumetric energy density.[1,2] However, DMFCs are plagued by several drawbacks, including the low boiling point and high toxicity of methanol, together with severe catalyst poisoning during long-term operation.[3,4] To address these issues, one can switch to alcohols with high molecular weights, such as ethylene glycol (EG) and glycerol that feature high boiling points and low toxicity.[5] With regard to the catalyst, an effective strategy is to incorporate Ru into the conventional Pd catalysts for the formation of a Pd-Ru alloy. The alloy-based catalysts are capable of not only enhancing the activity by modulating the electronic structure but also significantly improving the durability owing to the increased resistance to CO poisoning.[6–8] Additionally, compared with other precious metals such as Pt and Rh, Ru has a relatively high abundance in the Earth's crust and its current price is about three times lower than those of Pt and Rh, making it promising for the large-scale use in commercial applications.[9] However, Pd and Ru take completely different crystal structures in the bulk, face-centered cubic (fcc) for Pd versus hexagonal close-packed (hcp) for Ru, and their reduction potentials also show significant difference (Pd^{2+}/Pd: 0.95 V vs the standard hydrogen electrode (SHE); Ru^{3+}/Ru: 0.39 V vs SHE), making it challenging to synthesize Pd-Ru alloy catalysts with controllable compositions and structures. Thus far, the Pd-Ru catalysts reported in literature were mainly based on irregular nanoparticles, and nanoflowers or nanobranches featuring a low content of Ru.[10–18]

As an alternative to the conventional catalysts based upon solid nanoparticles, nanocages have recently emerged as an intriguing class of catalysts for various reactions.[19–25] The characteristic hollow structure, ultrathin and porous walls of nanocages are advantageous in maximizing the atom utilization efficiency while the well-controlled surface structures could be leveraged to optimize the active sites.[26,27] One effective route to the synthesis of nanocages is based upon galvanic replacement, which involves the spontaneous reduction of metal ions at the expense of oxidation of a sacrificial template.[28] Moreover, galvanic replacement can be completed within a short period, making it attractive for practical applications.[29–31] Regarding the synthesis of Pd-Ru nanocages, despite the well-established protocols for the production of Pd nanocrystals with diverse

Dr. M. Zhao, Z. Lyu, M. Xie, Dr. Z. D. Hood, Prof. Y. Xia
School of Chemistry and Biochemistry
Georgia Institute of Technology
Atlanta, GA 30332, USA
E-mail: younan.xia@bme.gatech.edu
Dr. Z. D. Hood, Dr. M. Chi
Center for Nanophase Materials Sciences
Oak Ridge National Laboratory
Oak Ridge, TN 37831, USA
Z. Cao, Prof. Y. Xia
The Wallace H. Coulter Department of Biomedical Engineering
Georgia Institute of Technology and Emory University
Atlanta, GA 30332, USA
The ORCID identification number(s) for the author(s) of this article can be found under https://doi.org/10.1002/smtd.201900843.

DOI: 10.1002/smtd.201900843

shapes, the galvanic replacement between Pd and Ru(III) ions is not thermodynamically favorable.[32] Additionally, the lack of Ru nanocrystals with well-defined shapes creates a barrier to the shape-controlled synthesis of Pd-Ru nanocages via the galvanic replacement between Ru and Pd(II) ions.[33,34] Recently, our group discovered that the presence of Br^- ions could trigger the galvanic replacement between Pd cubes and Ru(III) ions, opening a new avenue for the production of Pd-Ru bimetallic nanocrystals. The generated Ru atoms were preferentially deposited on the edges and corners of the Pd seeds, giving rise to the formation of Pd-Ru core-frame nanocrystals.[35]

In the present work, we intentionally introduced I^- ions into the synthesis to facilitate ligand exchange with Pd(II) ions for the formation of PdI_4^{2-} ions, a precursor with a reduction potential as low as 0.18 V versus SHE.[36] The dramatical decrease in reduction potential makes it viable to initiate the galvanic replacement between Pd and Ru(III) ions. Upon mixing Pd nanocubes with Ru(III) precursor in the presence of I^- ions, Pd-Ru nanocages featuring a cubic shape and a wall thickness of ≈2.5 nm could be obtained within 20 min. Significantly, the packing of Ru atoms in the walls of the nanocages followed an fcc structure instead of the hcp lattice adopted by bulk Ru. Quantitative study was conducted to investigate the effect of I^- ions on the reduction kinetics of Ru(III) ions throughout the synthesis. Additionally, we could readily control the size of the nanocages in the range of 6–18 nm by leveraging Pd seeds with different edge lengths. When benchmarked against the commercial Pd/C catalyst, the Pd-Ru alloy nanocages exhibited greatly enhanced activity and durability toward both EG and glycerol oxidation reactions (EGOR and GlyOR).

2. Results and Discussion

The synthesis started with the preparation of Pd nanocubes that were 18 nm in edge length (Figure S1, Supporting Information), which then served as the sacrificial templates. The as-synthesized Pd templates were then mixed with poly(vinylpyrrolidone) (PVP), sodium iodide (NaI), and Ru(III) precursor in triethylene glycol (TEG), and heated at 180 °C for 20 min. **Figure 1**a,b, shows high-angle annular dark-field scanning transmission electron microscopy (HAADF-STEM) images of the resultant Pd-Ru nanocrystals, from which the hollow interiors and cubic shape could be well resolved. The average wall thickness of the nanocages was calculated to be ≈2.5 nm. According to the atomic-resolution STEM image in Figure 1c, the lattice fringe spacing of 1.9 Å could be assigned to the {200} planes of an fcc Pd-Ru alloy, implying that Ru atoms in the Pd-Ru nanocages were crystallized in an fcc phase rather than the hcp lattice intrinsic to bulk Ru.[34] The fcc phase was further confirmed by X-ray diffraction (XRD) analysis (Figure S2, Supporting Information). The characteristic peaks were positioned between those of fcc-Pd and fcc-Ru, suggesting an fcc phase and an alloy structure. Based on the energy-dispersive X-ray (EDX) spectroscopy mapping analysis (Figure 1d), both Pd and Ru were uniformly distributed in the wall of the nanocage, confirming the formation of an alloy structure. The weight percentages of Pd and Ru in the nanocages were derived as 62.2 and 37.8 wt%, respectively, corresponding to an atomic ratio of 61:39 (denoted: $Pd_{61}Ru_{39}$).

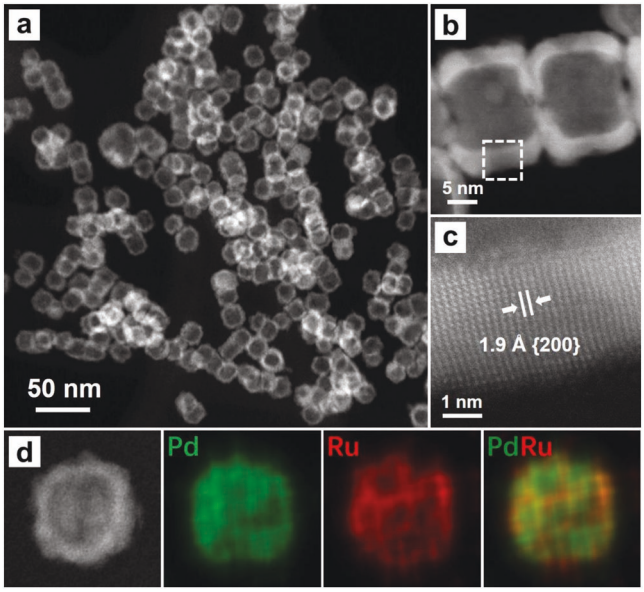

Figure 1. HAADF-STEM images of a) the Pd-Ru nanocages prepared using the standard protocol and b) two nanocages at a higher magnification. c) Atomic-resolution STEM image taken from the edge region marked by a box in panel (b). d) HAADF-STEM and EDX mapping (Pd, green and Ru, red) images of an individual Pd-Ru nanocage.

Figure S3 (Supporting Information) shows the XPS spectra recorded from the 18 nm Pd cubic seeds and the as-synthesized Pd-Ru nanocages. After the galvanic replacement reaction, the binding energies of Pd $3d_{3/2}$ and $3d_{5/2}$ changed from 340.42 and 335.13 eV for the Pd cubic seeds to 340.57 and 335.28 eV for the nanocages, respectively, suggesting a upshift of 0.15 eV. The change of binding energy clearly indicates that the alloying of Pd with Ru could effectively modulate the electronic structure of Pd (Figure S3a,b, Supporting Information). Figure S3c (Supporting Information) shows the binding energies of Ru $3d_{3/2}$ and $3d_{5/2}$, which were derived as 283.88 and 279.92 eV, respectively, revealing the metallic state of Ru in the products. The binding energy of Ru $3p_{3/2}$ was positioned at 461.38 eV, further confirming the presence of metallic Ru in the nanocages (Figure S3d, Supporting Information).

The formation mechanism of Pd-Ru nanocages was investigated by conducting electron microscopy analysis on the intermediates collected at different stages into a standard synthesis (**Figure 2**). In the initial stage (t = 5 min, Figure 2a), the surface of the Pd cubic seeds became bumpy owing to the generation of small pits. At t = 10 min, the small pits evolved into pinholes while the concave surface was filled owing to the co-deposition of Pd and Ru atoms (Figure 2b). After the reaction had proceeded for 15 min, the pinholes became enlarged, growing more deeply into the Pd templates (Figure 2c). Eventually, Pd-Ru nanocages characterized by hollow interiors and a cubic shape were obtained after 20 min into the synthesis (Figure 2d). After reaction, the conversion of Pd seeds into the nanocages was determined to be as high as 80.6%. The formation pathway of the nanocages clearly suggested the involvement of galvanic replacement between Pd nanocubes and Ru(III) ions. Since the standard reduction potential of Pd^{2+}/Pd pair (0.95 V vs SHE) is much greater than that

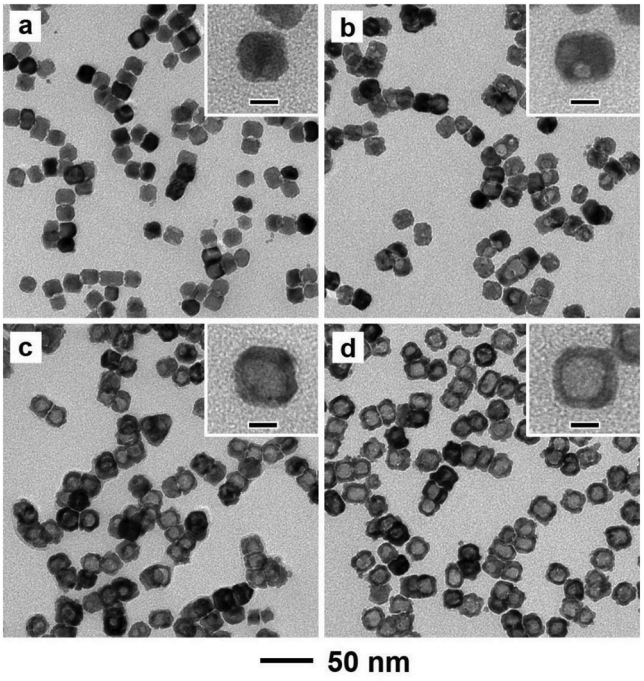

Figure 2. TEM images of the intermediate products obtained at different stages into a standard synthesis: a) 5, b) 10, c) 15, and d) 20 min, respectively. The insets show TEM images of individual nanocrystals at a higher magnification. The scale bars in the insets are 10 nm.

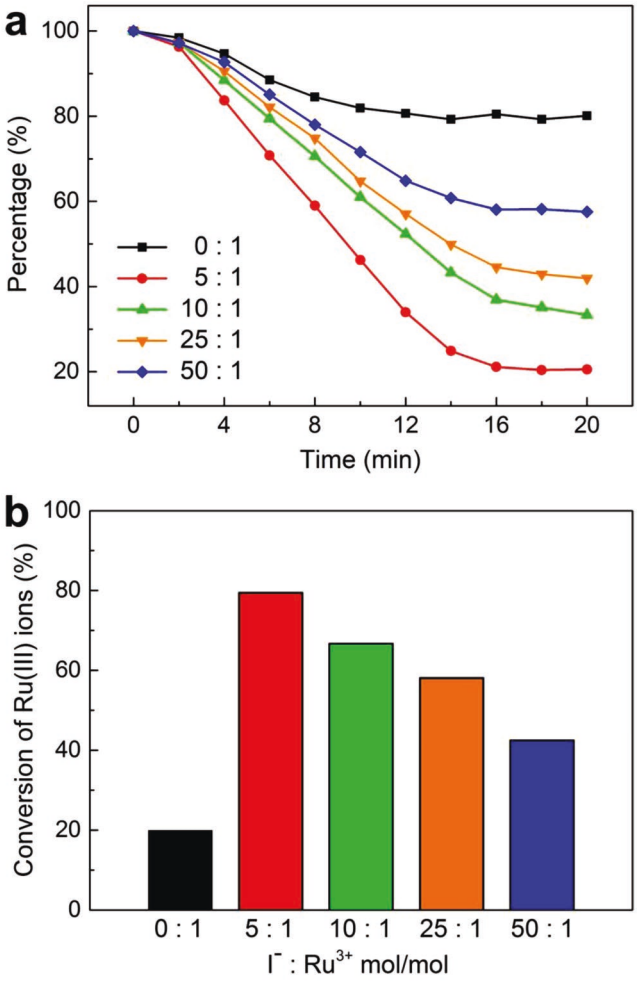

Figure 3. Quantitative analysis of the reduction kinetics of Ru(III) ions involved in the syntheses of Pd-Ru nanocages under different reaction conditions. Plots showing a) the reduction kinetics and b) normalized conversion of Ru(III) ions conducted by following the standard protocol except for the variation in I^- to Ru^{3+} ratio.

of Ru^{3+}/Ru pair (0.39 V vs SHE),[32] the galvanic replacement between Pd and Ru(III) ions is not favored by thermodynamics under the standard conditions. However, when I^- ions were added into the synthesis, Pd(II) and I^- ions could undergo ligand exchange to form PdI_4^{2-} ions, leading to a dramatic drop in the reduction potential (PdI_4^{2-}/Pd: 0.18 V vs SHE).[36] Although the presence of halide ions has also been reported to slightly slow down the reduction of Ru(III) ions, the successful initiation of galvanic replacement between Pd and Ru(III) ions suggested that the effect of I^- ions on the reduction potential of Ru(III) ions was not as notable as the case of Pd(II) ions.[24,25] During the reaction, the Pd atoms were spontaneously oxidized and dissolved into the solution in the form of PdI_4^{2-} ions and simultaneously, Ru(III) ions were reduced to Ru atoms for their deposition on the Pd templates. Additionally, the formed PdI_4^{2-} ions would also be reduced to generate Pd atoms and collectively deposited on the seeds with Ru atoms, giving rise to the formation of a Pd-Ru alloy.

Given that galvanic replacement was enabled by the addition of I^- ions, we varied the amount of I^- ions while fixing the amount of Ru(III) precursor to examine the role of I^-/Ru^{3+} ratio in the formation of Pd-Ru nanocages. Figure S4a (Supporting Information) shows the Pd-Ru nanocrystals obtained using the standard protocol except for the absence of I^- ions. The products possessed a cubic shape and were covered by small nanoparticles on the surface. When the I^-/Ru^{3+} ratio was 5:1, the resultant Pd-Ru nanocrystals were characterized by hollow interiors (Figure S4b, Supporting Information). However, their surfaces became rough relative to the standard sample, indicating fast deposition over surface diffusion of Ru and Pd atoms. As the I^-/Ru^{3+} ratio was increased to 25:1, a majority of the as-synthesized nanocrystals had a hollow structure and a cubic shape, whereas some of the nanocages possessed smaller hollow interiors relative to the standard sample (Figure S4c, Supporting Information). If the I^-/Ru^{3+} ratio was set to 50:1, the products contained both solid and hollow nanocrystals (Figure S4d, Supporting Information). Noticeably, the hollow interiors in the products were further shrunken in contrast to the sample shown in Figure S4c (Supporting Information), implying suppressed galvanic replacement. Taken together, the addition of I^- ions was essential to the initiation of the galvanic replacement reaction between Pd and Ru(III) ions, which could be promoted or retarded by decreasing or increasing the I^-/Ru^{3+} ratio.

We also conducted a quantitative study of the reduction kinetics of Ru(III) ions involving different I^-/Ru^{3+} ratios to elucidate the effect of I^- ions on the formation of Pd-Ru nanocages (**Figure 3**a). When the I^-/Ru^{3+} ratio was varied in the range of 0–50, the consumption of Ru(III) ions showed similar trends throughout the reaction, which quickly dropped within the

first 16 min and then became steady in the following stage. Despite the similar trends, the instantaneous consumption and final conversion of Ru(III) ions at various I^-/Ru^{3+} ratios differed remarkably from each other (Figure 3). In the absence of I^- ions, the Ru(III) ions were consumed at a slow rate, ending up with a conversion of only 19.9%. In comparison, when the I^-/Ru^{3+} ratio was 5:1, the Ru(III) ions were depleted very quickly, resulting in a conversion as high as 79.4%. This result was consistent with the electron microscopy analysis shown in Figure S4b (Supporting Information), in which the rough surface suggested fast deposition of Ru atoms. For the standard synthesis with an I^-/Ru^{3+} ratio of 10:1, 66.7% of the Ru(III) ions had been consumed after reaction for 20 min (Figure 3b), lower than what was involved at an I^-/Ru^{3+} ratio of 5:1. As the I^-/Ru^{3+} ratio was further increased to 25:1 and 50:1, the consumption of Ru(III) ions was decelerated relative to that of the standard synthesis, resulting in conversions of 58.0% and 42.4%, respectively (Figure 3b). This trend was in agreement with our prior work, where the presence of Br^- ions was found to retard the reduction of Ru(III) ions.[23–25] Altogether, our kinetic study suggested that the reduction of Ru(III) ions was facilitated upon the addition of I^- ions into the synthesis but then retarded as the atomic ratio of I^-/Ru^{3+} was increased.

Figure S5 (Supporting Information) shows the products prepared using the standard protocol except for the variation in the amount of Ru(III) precursor. When 0.4 mg of Ru(III) precursor was used, the products showed hollow interiors smaller than those of the standard sample (Figure S5a, Supporting Information). Based on the composition analysis (Table S1, Supporting Information), the atomic ratio of Pd/Ru in the nanocages was 79:21 (denoted $Pd_{79}Ru_{21}$). If 0.6 mg of Ru(III) precursor was added into the synthesis, the galvanic replacement between Pd and Ru(III) ions was accelerated, leading to an increase in the reduction rate of Ru(III) ions and thereby an enhanced deposition rate for the Ru atoms. As a consequence, the resultant nanocages showed a bumpy surface (Figure S5b, Supporting Information), together with a Pd/Ru ratio of 59:41 (denoted as $Pd_{59}Ru_{41}$, Table S1, Supporting Information). If 0.7 and 0.8 mg of Ru(III) precursor were used, both of the products displayed a nanocage structure while the surface roughness became increasingly significant, corresponding to compositions of 57:43 and 55:45, respectively, in term of Pd/Ru ratio (Figure S5c,d and Table S1, Supporting Information; denoted $Pd_{57}Ru_{43}$ and $Pd_{55}Ru_{45}$, respectively).

We also characterized the Pd-Ru nanocages with variable compositions using XRD to determine the crystal phase. As shown in **Figure 4**, the diffraction peaks of all the samples were located between those of fcc-Pd and fcc-Ru, indicating that the nanocrystals were made of fcc-structured Pd-Ru alloys. Noticeably, the Ru atoms in the alloy nanocages followed an fcc packing, distinctive from their bulk state featuring an hcp lattice. The formation of fcc-Ru could be attributed to the template effect exerted by Pd templates, which directed the deposited Ru atoms to follow the arrangement of the underlying Pd atoms.[23–25,35,37] Specifically, for sample $Pd_{79}Ru_{21}$, its characteristic peaks were left shifted compared with those of the standard sample owing to the increased proportion of Pd in the nanocages.[38] In contrast, as the proportion of Ru was gradually increased in $Pd_{59}Ru_{41}$, $Pd_{57}Ru_{43}$, and $Pd_{55}Ru_{45}$, their

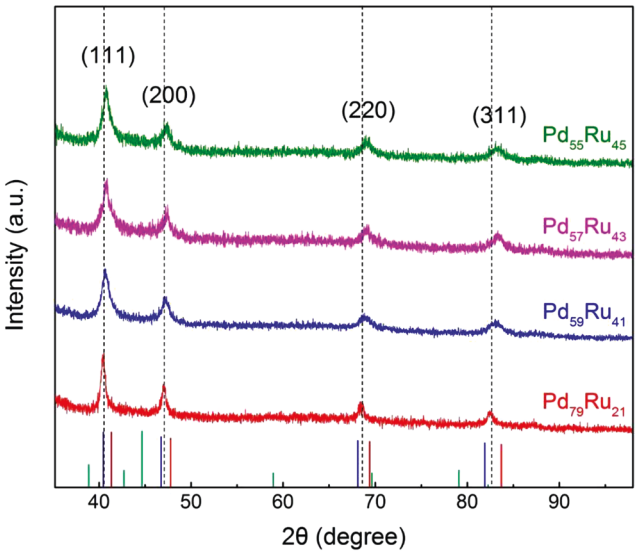

Figure 4. XRD patterns of the Pd-Ru nanocages with different elemental compositions. The characteristic peaks of fcc-Pd, fcc-Ru, and hcp-Ru are marked by blue, red, and green lines, respectively, at the bottom. The characteristic peaks of the standard sample ($Pd_{61}Ru_{39}$) are marked by the black dashed lines.

characteristic peaks displayed a right shift relative to those of the standard sample (Figure 4). It should be pointed out that the characteristic peaks of $Pd_{79}Ru_{21}$ were sharper relative to those of other three samples (Figure 4), which can be rationalized by both the higher content of Pd and the larger particle size. As shown in Figure S5a (Supporting Information), the particle size (i.e., wall thickness) of $Pd_{79}Ru_{21}$ is much larger than the samples shown in Figure S5b–d (Supporting Information) owing to the incomplete extraction of Pd seeds via galvanic replacement. With regard to $Pd_{59}Ru_{41}$, $Pd_{57}Ru_{43}$, and $Pd_{55}Ru_{45}$, although the decreased content of Pd would result in reduced sharpness for the diffraction peaks, their average wall thicknesses, however, show a gradual increase owing to the introduction of an increased amount of the Ru(III) precursor. As a result, the increase in sharpness for the diffraction peaks, as caused by the higher Pd content in the alloy, became insignificant (Figure 4).

For galvanic replacement, the size of the sacrificial template essentially defines the dimension of the product. To tune the size of Pd-Ru nanocages, we employed Pd nanocubes with edge lengths of 6 and 10 nm (Figure S6a,b, Supporting Information) as templates to conduct the synthesis while keeping other reaction conditions same as the standard protocol. Figure S6c,d (Supporting Information) shows the Pd-Ru nanocrystals prepared from 6 and 10 nm Pd cubes, respectively, both displaying a nanocage structure. For the nanocages prepared from 6 nm Pd cubes, the cubic shape was slightly deformed. This observation could be rationalized by the fast reaction rate arising from the high surface-to-volume ratio of small seeds and thus an increased number of active sites for galvanic replacement (Figure S6c, Supporting Information). In contrast, when 10 nm Pd cubes served as seeds, the resultant nanocages possessed well-defined cubic shape and a relatively smooth surface (Figure S6d, Supporting Information). The compositions of the 6 and 10 nm nanocages were derived as 57:43 and 58:42,

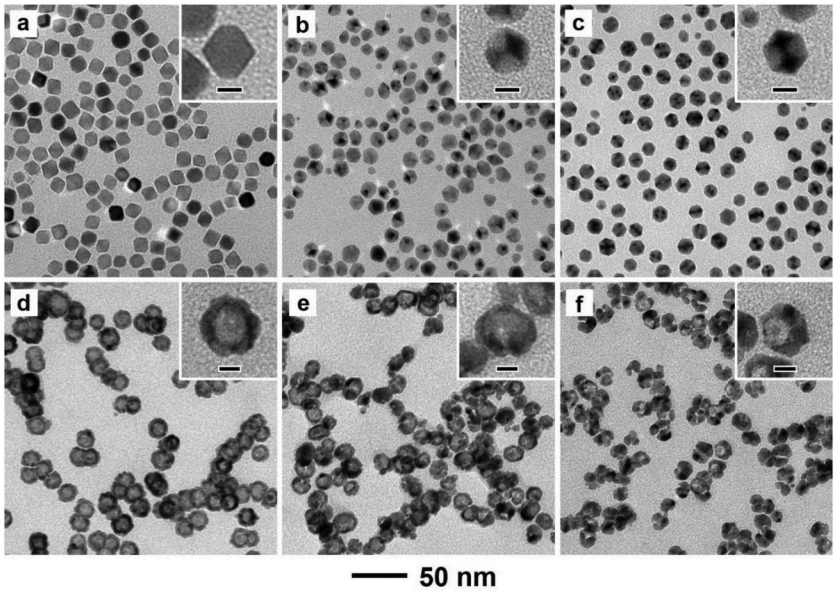

Figure 5. TEM images of different types of Pd polyhedra and the corresponding Pd-Ru hollow nanocrystals derived from them: a,d) 15 nm octahedra, b,e) 14 nm decahedra, and c,f) 12 nm icosahedra. The insets show TEM images of individual hollow nanocrystals at a higher magnification. The scale bars in the insets are 10 nm.

respectively, in terms of Pd/Ru ratio, slightly greater than that of the standard sample (Pd/Ru = 61:39). The increased proportion of Ru in the smaller nanocages could be attributed to the enhanced activity of smaller Pd seeds toward galvanic replacement, leading to a greater conversion for Ru(III) ions. Taken together, by employing Pd seeds with different edge lengths, we could readily tune the size of the Pd-Ru nanocages in the range of 6–18 nm.

We also attempted to extend our synthetic protocol to Pd seeds with different shapes including octahedral, decahedral, and icosahedral, which were enclosed by 8 {111} facets, 10 {111} facets plus 10 twin boundaries, and 20 {111} facets plus 30 twin boundaries, respectively (**Figure 5**a–c). When Pd octahedra were used, the as-synthesized nanocrystals featured hollow interiors (Figure 5d). However, their surfaces were not covered by well-defined {111} facets owing to the strong binding of I^- ions to {100} facets.[39] When Pd decahedra served as the templates, Pd-Ru nanocages with very rough surfaces were obtained, which could be ascribed to the enhanced galvanic replacement stemming from the presence of highly active twin boundaries (Figure 5e).[40,41] The effect of twin boundaries was further confirmed by leveraging Pd icosahedra with an increased density of twin boundaries as the templates. As shown in Figure 5f, the edges of most of the particles were deformed and the icosahedral shape was also largely lost.[42–44]

We also evaluated the catalytic performance of the Pd-Ru alloy nanocages prepared using 18 nm Pd cubic seeds (i.e., sample $Pd_{61}Ru_{39}$) and benchmarked against the commercial Pd/C and Ru/C catalysts toward EGOR and GlyOR. The as-synthesized Pd-Ru nanocages and Ru nanoparticles were loaded on carbon support with a weight percentage of ≈20 wt% in terms of metal contents prior to electrochemical measurements (Figures S7 and S8, Supporting Information). When leveraging Ru/C as the catalyst, no oxidation peaks of EG and glycerol were observed, except for the presence of oxygen evolution reaction peaks, suggesting the inertness of Ru in catalyzing EGOR and GlyOR (Figure S8, Supporting Information). **Figure 6**a shows the cyclic voltammograms (CVs) curves recorded in an aqueous mixture of 1.0 M KOH and 1.0 M EG at a scanning rate of 50 mV s^{-1}, from which the Pd mass-normalized peak currents (i.e., mass activities) were derived as 5.54 and 1.09 A mg_{Pd}^{-1} for the Pd-Ru nanocages and commercial Pd/C, respectively. Significantly, the nanocages exhibited a 5.1-fold enhancement in terms of mass activity relative to the commercial Pd/C catalyst. The durability was examined by subjecting the catalysts to electrochemical cycling, as summarized in Figure 6b. After 1000 cycles of accelerated durability test, the mass activity of the Pd-Ru nanocages decreased to 3.60 A mg_{Pd}^{-1}, but it was still 3.3 times greater than that of the pristine commercial Pd/C and 17.1-fold as high as that of the Pd/C catalyst (0.21 A mg_{Pd}^{-1}) undergoing the same durability test. In particular, the mass activity of the nanocages indicated a decay of 35.1% while 80.6% drop from the initial value was observed for the commercial Pd/C catalyst, demonstrating the enhanced durability of the Pd-Ru nanocages toward EGOR.

Figure 6c shows the Pd mass-normalized CV curves of the Pd-Ru nanocages and the commercial Pd/C measured in an aqueous solution containing 1.0 M KOH and 1.0 M glycerol. Specifically, the Pd-Ru nanocages exhibited a mass activity of 6.27 A mg_{Pd}^{-1}, which is 6.2-fold greater than that of the commercial Pd/C catalyst (1.01 A mg_{Pd}^{-1}). After 1000 cycles of accelerated durability test, the mass activity of the nanocages was still at 3.71 A mg_{Pd}^{-1}, whereas that of the commercial Pd/C catalyst dramatically dropped to 0.20 A mg_{Pd}^{-1}. In particular, the mass activity of tested nanocages was 3.7 and 17.6 times greater than that of the commercial Pd/C catalyst before and after accelerated durability test, respectively (Figure 6d). Noticeably, the mass activities of the Pd-Ru nanocages and commercial Pd/C indicated drops of 40.8% and 79.2% after 1000 electrochemical cycles, respectively, confirming the superior durability of Pd-Ru nanocages toward GlyOR.

We note that recent studies suggested the possible dissolution of the Pt counter electrode during electrochemical measurements, which would then be deposited on the catalyst to affect its performance.[45,46] Based on the inductively coupled plasma mass spectrometry (ICP-MS; with sensitivity on the level of parts per billion) analysis, the atomic ratios of Pt and Pd in the tested catalysts for both EGOR and GlyOR were lower than 0.01%, suggesting that the deposition of Pt on the catalyst was not be a major concern in our electrochemical measurements. We also characterized the Pd-Ru nanocages after accelerated durability test to assess their stability in terms of shape and crystal phase. As shown in Figures S9 and S10 (Supporting Information), both the cubic shape and fcc phase of the

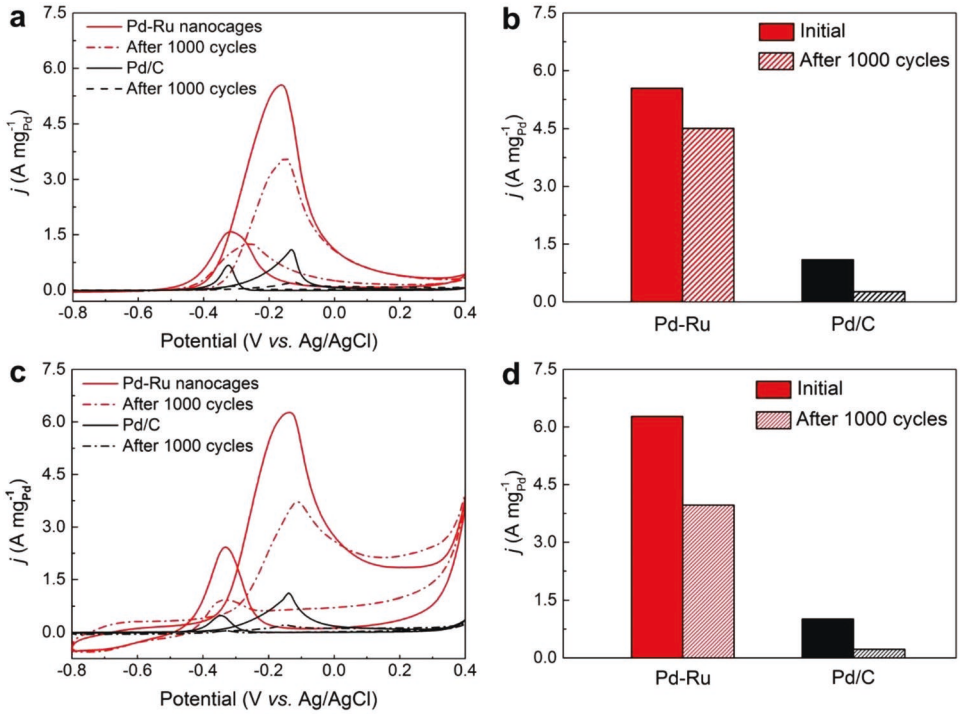

Figure 6. Comparison of the catalytic performance of the Pd-Ru nanocages prepared using the standard protocol and the commercial Pd/C catalyst toward EGOR and GlyOR. a) Pd mass-normalized CV curves of the nanocages and commercial Pd/C measured before and after 1000 cycles of accelerated durability test toward EGOR. b) Summary of the mass activities of the nanocages and commercial Pd/C before and after 1000 CV cycles of accelerated durability test. c) Pd mass-normalized CV curves of the nanocages and commercial Pd/C measured before and after 1000 CV cycles of accelerated durability test toward GlyOR. d) Summary of mass activities of the nanocages and commercial Pd/C before and after 1000 CV cycles of accelerated durability test.

nanocages could be well preserved after the accelerated durability test. Moreover, the compositions of catalysts tested for EGOR and GlyOR were derived as 60:40 and 59:41, respectively, in terms of the Pd/Ru ratio, with essentially no obvious change relative to that of the pristine nanocages (Pd/Ru = 61:39).

The enhancements in mass activity and durability of the Pd-Ru nanocages could be ascribed to the nanocage structure and ligand effect stemming from the alloying of Pd and Ru.[47–49] On one hand, the hollow interiors, ultrathin (i.e., 2.5 nm) and porous walls of Pd-Ru nanocages could substantially increase the utilization efficiency of metal atoms and thereby boosting the mass activity.[18,22] On the other hand, the ligand effect arising from Pd and Ru alloying was instrumental to modulating the electronic structure for the generation of an alloy surface favorable for C—C bond cleavage of alcohol molecules, electronic charge transfer, and desorption of carbonate intermediates.[50] Additionally, in contrast to the commercial Pd nanoparticles which were enclosed by a mix of {100} and {111} facets, the as-synthesized Pd-Ru nanocages were predominantly covered by {100} facets. The {100} facets have been demonstrated to be more active than {111} facets toward alcohol oxidation, which could bind more strongly to alcohol molecules and thus facilitating the C—C bond scission.[51,52] With regard to the durability, the presence of Ru atoms in the nanocages could greatly mitigate CO poisoning of the catalysts by reducing the adsorption energy of CO on the metal surface, which is advantageous to the removal of CO.[53–56] In particular, Ru atoms in an fcc packing have been reported to exhibit superior performance than their hcp counterpart toward CO oxidation, thus facilitating the removal of CO via oxidation.[57] As such, the nanocages could expose more active sites than the commercial Pd/C catalyst for catalyzing the oxidation of alcohol molecules during the long-term operation, giving rise to the enhanced durability toward both EGOR and GlyOR.

3. Conclusion

We have demonstrated a facile route to the synthesis of Pd-Ru nanocages based upon the I^--assisted galvanic replacement between Pd and Ru(III) ions. The as-synthesized nanocages showed a cubic shape and an ultrathin wall thickness of roughly 2.5 nm. Quantitative analysis suggested that the I^-/Ru^{3+} ratio significantly affected the reduction kinetics of Ru(III) ions, which needs to be controlled to ensure the complete removal of the Pd template and the formation of a smooth surface. Interestingly, the walls of the nanocages were made of a Pd-Ru alloy, with the Ru atoms crystallized in an fcc phase rather than the hcp phase intrinsic to bulk Ru. The synthetic protocol could also be extended to Pd cubes with different edge lengths, by which the size of the nanocages could be readily tuned in the range of 6–18 nm. When explored as an electrocatalyst toward both EGOR or GlyOR, the Pd-Ru nanocages exhibited substantially enhanced activity and durability relative

to the commercial Pd/C catalyst. We believe our work offers an effective method for the facile synthesis of fcc-structured Pd-Ru alloy nanocages through galvanic replacement, together with an insight into their enhanced catalytic performance.

4. Experimental Section

Chemicals and Materials: EG (99%) was purchased from J. T. Baker. Diethylene glycol (DEG, 99%), TEG (99%), glycerol (99%), sodium tetrachloropalladate(II) (Na_2PdCl_4, 99.99%), formaldehyde (HCHO, 36.5–38%), sodium sulfate (Na_2SO_4, 99%), PVP (55 000 in average M.W.), potassium bromide (KBr, 99%), L-ascorbic acid (AA, 99%), potassium chloride (KCl, 99%), potassium hydroxide (KOH), and NaI (99.5%) were all ordered from Sigma-Aldrich. Ruthenium(III) 2,4-pentaedionate ($Ru(acac)_3$, 24% Ru) was obtained from Alfa Aesar. The aqueous solutions were prepared using deionized (DI) water with a resistivity of 18.2 MΩ cm at room temperature.

Synthesis of Pd Cubes with Edge Lengths of 6, 10, and 18 nm: In a typical synthesis of 18 nm Pd cubes,[58] 8 mL of water containing KBr (600 mg), PVP (105 mg), and AA (60 mg) was transferred into a 20 mL vial and heated in an oil bath at 80 °C for 10 min. Meanwhile, 3 mL of an aqueous solution containing 57 mg of Na_2PdCl_4 was injected into the vial in one shot. After 3 h, the reaction was quenched in an ice-water bath. With respect to the syntheses of 6 and 10 nm Pd cubes, the same protocol was used except that the 600 mg KBr was replaced with a mixture of 5 mg of KBr and 185 mg of KCl, and 300 mg of KBr, respectively.

Synthesis of 15 nm Pd Octahedra: Typically,[59] a mixture containing water (8 mL), HCHO (50 µL), PVP (315 mg), and 6 nm Pd cubes (2.73 mg) was heated in an oil bath at 60 °C. After 10 min, 3 mL of an aqueous Na_2PdCl_4 solution (58.3 mg mL^{-1}) was added into the mixture in one shot. The reaction was continued for 3 h and then quenched in an ice-water bath. The solid products were collected by centrifugation and washed three times with water.

Synthesis of 14 nm Pd Decahedra: In a typical synthesis,[53] 2 mL of DEG solution containing 44 mg of Na_2SO_4 and 80 mg of PVP was heated in an oil bath at 105 °C for 10 min. Subsequently, 1 mL of DEG solution containing 15.5 mg of Na_2PdCl_4 was added into the mixture in one shot. After 3 h, the solid products were collected by centrifugation and washed once with acetone and twice with DI water.

Synthesis of 12 nm Pd Icosahedra: Typically,[60] 2 mL of DEG solution containing PVP (80 mg) was heated in an oil bath at 130 °C for 10 min. Subsequently, 1 mL of DEG containing Na_2PdCl_4 (15.5 mg) was injected into the mixture in one shot. After 3 h, the solid products were collected by centrifugation and washed once with acetone and twice with DI water.

Synthesis of 3 nm Ru Nanoparticles: In a typical synthesis, 50 mg of PVP and 7.5 mg of $Ru(acac)_3$ were dissolved in 5 mL of EG. The mixture was then heated to 180 °C for 2 h under magnetic stirring. The solid products were collected by centrifugation and washed three times with DI water.

Synthesis of Pd-Ru Nanocages: In a standard synthesis, 0.25 mg of 18 nm Pd cubes, 12.5 mg of PVP, 2 mg of NaI, 0.5 mg of $Ru(acac)_3$ (I^-:Ru^{3+} = 10:1 mol/mol), and 2.5 mL of TEG were mixed in a 20 mL vial. The vial was tightly capped and then placed in an oil bath heated at 180 °C. After 20 min, the solid products were collected by centrifugation and washed once with acetone and twice with DI water.

Characterization: TEM images were acquired on a Hitachi 7700 microscope. HAADF-STEM images and EDX spectroscopy data were acquired on an aberration-corrected Hitachi HD2700 STEM at the Institute for Electronics and Nanotechnology (IEN, Georgia Institute of Technology) and a Cs-corrected FEI Titan 80/300 kV TEM/STEM at Oak Ridge National Laboratory (ORNL). The metal contents in various samples were analyzed using ICP-MS (NexION 300Q, PerkinElmer). XRD patterns were recorded with a PANalytical X'Pert PRO Alpha-1 diffractometer using 1.8 kW Ceramic Copper tube source.

Quantitative Analysis of the Reduction Kinetics: In a typical procedure, 50 µL was sampled from the reaction mixture every 2 min and then quickly quenched in an ice-water bath. The aliquot was mixed with 950 µL of acetone to precipitate out the solid particles, followed by centrifugation. The supernatant was collected and then diluted to a concentration suitable for ICP-MS analysis.

Electrochemical Measurements: An electrochemical workstation (CHI 600E potentiostat) was used to carry out all the electrochemical measurements in a three-electrode cell. A Ag/AgCl electrode and a Pt mesh served as the reference and counter electrodes, respectively. A Luggin capillary was used to allow sensing of the solution potential close to the working electrode without adverse effects. The as-synthesized Pd-Ru nanocages were loaded on a carbon support (Ketjenblack EC-300J, AkzoNobel) and used as working electrode. The weight percentage of the total amount of both metals in the carbon-supported catalyst is ≈20 wt%. CVs were recorded in an aqueous mixture of 1.0 M EG or glycerol and 1.0 M KOH, in the potential range of −0.8 to 0.4 V and at a scanning rate of 50 mV s^{-1}.

Supporting Information

Supporting Information is available from the Wiley Online Library or from the author.

Acknowledgements

This work was supported in part by the National Science Foundation (NSF) (CHE-1804970) and startup funds from the Georgia Institute of Technology. XRD and electron microscope analyses were conducted at the Institute for Electronics and Nanotechnology (IEN, Georgia Institute of Technology), a member of the National Nanotechnology Coordinated Infrastructure, which is supported by the NSF (ECCS-1542174). Part of the electron microscopy analyses was carried out in the Center for Nanophase Materials Sciences, which is a DOE Office of Science User Facility (M.C. and Z.D.H.). Z.D.H. gratefully acknowledges support from the NSF Graduate Research Fellowship (DGE-1650044) and the Georgia Tech-ORNL Fellowship.

Conflict of Interest

The authors declare no conflict of interest.

Keywords

electrocatalysis, face-centered cubic alloys, galvanic replacements, Pd-Ru nanocages, reduction kinetics

Received: December 8, 2019
Revised: January 10, 2020
Published online: January 29, 2020

[1] N. P. Brandon, S. Skinner, B. C. H. Steele, *Annu. Rev. Mater. Res.* **2003**, *33*, 183.
[2] X. Liu, J. Xi, B. Xu, B. Fang, Y. Wang, M. Bayati, K. Scott, C. Gao, *Small Methods* **2018**, *2*, 1800138.
[3] X. Zhao, M. Yin, L. Ma, L. Liang, C. Liu, J. Liao, T. Lu, W. Xing, *Energy Environ. Sci.* **2011**, *4*, 2736.
[4] A. Rabis, P. Rodriguez, T. J. Schmidt, *ACS Catal.* **2012**, *2*, 864.
[5] A. Serov, C. Kwak, *Appl. Catal., B* **2010**, *97*, 1.
[6] C. Bianchini, P. K. Shen, *Chem. Rev.* **2009**, *109*, 4183.

[7] A. Chen, C. Ostrom, *Chem. Rev.* **2015**, *115*, 11999.
[8] K. Kusada, H. Kobayashi, R. Ikeda, Y. Kubota, M. Takata, S. Toh, T. Yamamoto, S. Matsumura, N. Sumi, K. Sato, K. Nagaoka, H. Kitagawa, *J. Am. Chem. Soc.* **2014**, *136*, 1864.
[9] Y. Xia, M. Zhao, X. Wang, D. Huo, *MRS Bull.* **2018**, *43*, 860.
[10] Q. Shao, K. Lu, X. Huang, *Small Methods* **2019**, *3*, 1800545.
[11] M. Tang, S. Mao, M. Li, Z. Wei, F. Xu, H. Li, Y. Wang, *ACS Catal.* **2015**, *5*, 3100.
[12] H. Wang, Y. Li, D. Yang, X. Qian, Z. Wang, Y. Xu, X. Li, H. Xue, L. Wang, *Nanoscale* **2019**, *11*, 5499.
[13] P. Bi, W. Hong, C. Shang, J. Wang, E. Wang, *RSC Adv.* **2016**, *6*, 12486.
[14] K. Zhang, D. Bin, B. Yang, C. Wang, F. Ren, Y. Du, *Nanoscale* **2015**, *7*, 12445.
[15] J. Guo, R. Chen, F. Zhu, S. Sun, H. M. Villullas, *Appl. Catal., B* **2018**, *224*, 602.
[16] Z. Xiong, H. Xu, S. Li, Z. Gu, B. Yan, J. Guo, Y. Du, *Appl. Surf. Sci.* **2018**, *427*, 83.
[17] R. Awasthi, R. N. Singh, *Carbon* **2013**, *51*, 282.
[18] S. Dash, N. Munichandraiah, *Electrochim. Acta* **2015**, *180*, 339.
[19] M. Zhao, X. Wang, X. Yang, K. G. Gilroy, D. Qin, Y. Xia, *Adv. Mater.* **2018**, *30*, 1809156.
[20] M. Nazemi, S. R. Panikkanvalappil, M. A. El-Sayed, *Nano Energy* **2018**, *49*, 316.
[21] J. Park, T. Kwon, J. Kim, H. Jin, H. Y. Kim, B. Kim, S. H. Joo, K. Lee, *Chem. Soc. Rev.* **2018**, *47*, 8173.
[22] H. Liu, J. Qu, Y. Chen, J. Li, F. Ye, J. Y. Lee, J. Yang, *J. Am. Chem. Soc.* **2012**, *134*, 11602.
[23] M. Zhao, L. Figueroa-Cosme, A. O. Elnabawy, M. Vara, X. Yang, L. T. Roling, M. Chi, M. Mavrikakis, Y. Xia, *Nano Lett.* **2016**, *16*, 5310.
[24] M. Zhao, A. O. Elnabawy, M. Vara, L. Xu, Z. D. Hood, X. Yang, K. D. Gilroy, L. Figueroa-Cosme, M. Chi, M. Mavrikakis, Y. Xia, *Chem. Mater.* **2017**, *29*, 9227.
[25] M. Zhao, L. Xu, M. Vara, A. O. Elnabawy, K. D. Gilroy, Z. D. Hood, S. Zhou, L. Figueroa-Cosme, M. Chi, M. Mavrikakis, Y. Xia, *ACS Catal.* **2018**, *8*, 6948.
[26] X. Tian, X. Zhao, Y. Su, L. Wang, H. Wang, D. Dang, B. Chi, H. Liu, E. J. M. Hensen, X. W. Lou, B. Y. Xia, *Science* **2019**, *366*, 850.
[27] K. D. Gilroy, X. Yang, S. Xie, M. Zhao, D. Qin, Y. Xia, *Adv. Mater.* **2018**, *30*, 1706312.
[28] X. Xia, Y. Wang, A. Ruditskiy, Y. Xia, *Adv. Mater.* **2013**, *25*, 6313.
[29] Y. Zhang, Y. Wu, D. Qin, *J. Mater. Chem. C* **2018**, *6*, 5353.
[30] X. Sun, X. Yang, Y. Zhang, Y. Ding, D. Su, D. Qin, *Nanoscale.* **2017**, *9*, 15107.
[31] Y. Yang, Q. Zhang, Z. Fu, D. Qin, *ACS Appl. Mater. Interfaces* **2014**, *6*, 5.
[32] H. Zhang, M. Jin, Y. Xiong, B. Lim, Y. Xia, *Acc. Chem. Res.* **2013**, *46*, 1783.
[33] G. Chen, J. Zhang, A. Gupta, F. Rosei, D. Ma, *New J. Chem.* **2014**, *38*, 1827.
[34] H. Ye, Q. Wang, M. Catalano, N. Lu, J. Vermeylen, M. J. Kim, Y. Liu, Y. Sun, X. Xia, *Nano Lett.* **2016**, *16*, 2812.
[35] M. Zhao, Z. D. Hood, M. Vara, K. D. Gilroy, M. Chi, Y. Xia, *ACS Nano* **2019**, *13*, 7241.
[36] Y. Holade, D. P. Hickey, S. D. Minteer, *J. Mater. Chem. A* **2016**, *4*, 17154.
[37] M. Zhao, Z. Chen, Z. Lyu, Z. D. Hood, M. Xie, M. Vara, M. Chi, Y. Xia, *J. Am. Chem. Soc.* **2019**, *141*, 7028.
[38] A. R. Denton, N. W. Ashcroft, *Phys. Rev. A* **1991**, *43*, 3161.
[39] M. Chen, B. Wu, J. Yang, N. Zheng, *Adv. Mater.* **2012**, *24*, 862.
[40] W. Niu, G. Xu, *Nano Today* **2011**, *6*, 265.
[41] S. Zhou, M. Zhao, T.-H. Yang, Y. Xia, *Mater. Today* **2019**, *22*, 108.
[42] H. Wang, S. Zhou, K. D. Gilroy, Z. Cai, Y. Xia, *Nano Today* **2017**, *15*, 121.
[43] Z. Fan, H. Zhang, *Acc. Chem. Res.* **2016**, *49*, 2841.
[44] H. Cheng, N. Yang, P. Lu, Z. Zhang, H. Zhang, *Adv. Mater.* **2018**, *30*, 1707189.
[45] J. G. Chen, C. W. Jones, S. Linic, V. R. Stamenkovic, *ACS Catal.* **2017**, *7*, 6392.
[46] P. P. Lopes, D. Strmcnik, D. Tripkovic, J. G. Connell, V. Stamenkovic, N. M. Markovic, *ACS Catal.* **2016**, *6*, 2536.
[47] B. Y. Xia, H. B. Wu, X. Wang, X. W. Lou, *J. Am. Chem. Soc.* **2012**, *134*, 13934.
[48] J. Sheng, J. Kang, Z. Hu, Y. Yu, X. Fu, R. Sun, C. Wong, *J. Mater. Chem. A* **2018**, *6*, 15789.
[49] J. Sheng, J. Kang, H. Ye, J. Xie, B. Zhao, X. Fu, Y. Yu, R. Sun, C. Wong, *J. Mater. Chem. A* **2018**, *6*, 3906.
[50] A. Mahata, K. S. Rawat, I. Choudhuri, B. Pathak, *J. Mater. Chem. A* **2016**, *4*, 12756.
[51] Z. Wu, B. Miao, E. Hopkins, K. Park, Y. Chen, H. Jiang, M. Zhang, C. Zhong, L. Wang, *J. Phys. Chem. C* **2019**, *123*, 20853.
[52] H. Wang, Z. Liu, *J. Am. Chem. Soc.* **2008**, *130*, 10996.
[53] B. Hammer, Y. Morikawa, J. K. Nørskov, *Phys. Rev. Lett.* **1996**, *76*, 2141.
[54] M. Gajdos, A. Eichler, J. Hafner, *J. Phys.: Condens. Matter* **2004**, *16*, 1141.
[55] J. Xie, Q. Zhang, L. Gu, S. Xu, P. Wang, J. Liu, Y. Ding, Y. Yao, C. Nan, M. Zhao, Y. You, Z. Zou, *Nano Energy* **2016**, *21*, 247.
[56] S. Alayoglu, A. U. Nilekar, M. Mavrikakis, B. Eichhorn, *Nat. Mater.* **2008**, *7*, 333.
[57] K. Kusada, H. Kobayashi, T. Yamamoto, S. Matsumura, N. Sumi, K. Sato, K. Nagaoka, Y. Kubota, H. Kitagawa, *J. Am. Chem. Soc.* **2013**, *135*, 5493.
[58] M. Jin, H. Liu, H. Zhang, Z. Xie, J. Liu, Y. Xia, *Nano Res.* **2011**, *4*, 83.
[59] L. Figueroa-Cosme, K. D. Gilroy, T.-H. Yang, M. Vara, J. Park, S. Bao, A. G. M. da Silva, Y. Xia, *Chem. - Eur. J.* **2018**, *24*, 6133.
[60] H. Huang, Y. Wang, A. Ruditskiy, H.-C. Peng, X. Zhao, L. Zhang, J. Liu, Z. Ye, Y. Xia, *ACS Nano* **2014**, *8*, 7041.